

# THEMIS observations of the Hanle effect in $C_2$ lines

A. Asensio Ramos<sup>1</sup> and J. Trujillo Bueno<sup>1,2</sup>

<sup>1</sup> Instituto de Astrofísica de Canarias, 38205, La Laguna, Tenerife, Spain  
e-mail: aasensio@iac.es; jtb@iac.es

<sup>2</sup> Consejo Superior de Investigaciones Científicas, Spain

**Abstract.** Analysis of the Hanle effect in solar molecular lines allows us to obtain empirical information on unresolved, tangled magnetic fields at subresolution scales in the (granular) upflowing regions of the ‘quiet’ solar photosphere. Here we show observations of scattering polarization in selected  $C_2$  lines at increasingly closer distances to the solar limb, pointing out that the ratio of polarization amplitudes between suitably chosen line pairs varies in a systematic way. We interpret this variation in terms of a microturbulent magnetic field of the order of a few gauss whose strength decreases with height in the solar atmosphere.

**Key words.** Magnetic fields — polarization — scattering — Sun: photosphere — Stars: magnetic fields

## 1. Introduction

It has been pointed out recently that the observed scattering polarization in very weak spectral lines, such as those observed by Stenflo & Keller (1997) and Gandorfer (2000) in MgH and  $C_2$ , is coming mainly from the (granular) upflowing regions of the solar photosphere (Trujillo Bueno, 2003; Trujillo Bueno, Shchukina, & Asensio Ramos, 2004). Therefore, the Hanle effect in such molecular lines can be used to obtain information on unresolved magnetic fields in the granular regions of solar surface convection.

To this end, a powerful diagnostic tool is the Hanle-effect line-ratio technique for the  $C_2$  lines of the Swan system (see Trujillo Bueno, Asensio Ramos, & Shchukina, 2006, for a de-

tailed presentation with a summary of the various applications that have been performed). The advantage of this technique is that one does not need to carry out complex radiative transfer modeling of the observed molecular scattering polarization, given that the strength of the hidden field can be simply obtained through a direct comparison between the linear polarization amplitude observed at the wavelength location of the  $P_2(J)$  or  $R_2(J)$  line under consideration (whose critical Hanle field,  $B_H = 1.137 \times 10^{-7} A_{ul} / g_{Lande}$ , should be high enough to really serve as a reference line) and at that of the ensuing  $P_3(J-1)$  or  $R_3(J-1)$  line (whose  $B_H$  values are of the order of a few G). Results of the application of this “differential Hanle-effect” technique to on-disk observations have been reported by Trujillo Bueno (2003), Faurobert & Arnaud (2003),

---

Send offprint requests to: A. Asensio Ramos

Trujillo Bueno et al. (2004), Berdyugina & Fluri (2004), and Trujillo Bueno et al. (2006). For example, Trujillo Bueno et al. (2004) applied it to C<sub>2</sub> lines with  $J > 20$  and inferred a mean field strength  $\langle B \rangle \approx 15$  G for the case of an exponential probability distribution function (PDF) of microturbulent fields, or  $\langle B \rangle \approx 7$  G for the simpler case of a single value microturbulent field. On the other hand, Berdyugina & Fluri (2004) and Faurobert & Arnaud (2003) reported instead  $\langle B \rangle \approx 15$  G for the case of a single value microturbulent field. The disagreement with the value of 7 G determined by Trujillo Bueno et al. (2004) for the same model can be explained when we consider that Berdyugina & Fluri (2004) and Faurobert & Arnaud (2003) overestimated the Einstein coefficients by a factor 2, overlooking the fact that  $\Lambda$ -doubling is not present in C<sub>2</sub> (see Herzberg, 1950).

Having shown that the Hanle effect in C<sub>2</sub> lines leads to a hidden magnetic field of the order of a few G, our next step has been to investigate how its strength varies with height in the solar atmosphere. To this end, we have chosen the R-triplet at 5140 Å that Berdyugina & Fluri (2004) used in their investigation. Although the critical Hanle field of the R<sub>2</sub>(13) line is only  $B_H \approx 40$  G, it can still be used as a reference line because the C<sub>2</sub> lines with  $J > 20$  indicated that most of the (granular) upflowing photospheric volume is occupied by weaker fields (Trujillo Bueno, 2003; Trujillo Bueno et al., 2004). The advantage of such R-triplet is that the R<sub>2</sub>(13) reference line is not blended with the R<sub>1</sub>(14) line, which makes it easier to detect any possible magnetic depolarization. The advantage of the C<sub>2</sub> lines with  $J > 20$  is that the critical field of their P<sub>2</sub>(R<sub>2</sub>) lines is  $B_H > 100$  G, while their disadvantage is that such good reference lines are blended with their corresponding P<sub>1</sub>(R<sub>1</sub>) lines.

## 2. The Hanle effect in C<sub>2</sub> lines: theory and modeling

The rotational lines of C<sub>2</sub> observed between 5080 Å and 5160 Å belong to the  $d^3\Pi_g - a^3\Pi_u$   $v=0-0$  electronic transition. The magnetic properties of this system of C<sub>2</sub> have

been investigated by Berdyugina & Solanki (2002), concluding that both the upper and lower electronic states belong to intermediate coupling schemes, although they rapidly approach Hund's case (b) for  $J \geq 10$ . In both levels, the transition to the Paschen-Back regime occurs for magnetic field strengths higher than 70 kG and, therefore, we can safely treat them in the Zeeman regime. Since the spin of both levels is  $S=1$ , each rotational level splits into three sublevels, labeled as  $F_1$  (the one with  $J=N+1$ ),  $F_2$  (the one with  $J=N$ ) and  $F_3$  (the one with  $J=N-1$ ). Therefore, if both levels belong to Hund's case (b), the structure of the band consists of three sub-bands:  $^3\Pi_0 - ^3\Pi_0$ ,  $^3\Pi_1 - ^3\Pi_1$ ,  $^3\Pi_2 - ^3\Pi_2$ .  $\Lambda$ -doubling is not present in this molecule because it is composed of two identical nuclei. As a consequence, since the total wavefunction has to be symmetric under the exchange of the two nuclei, only one of the  $\Lambda$ -doubling levels is possible for each state. The allowed levels have parity – for the lower electronic state and parity + for the upper electronic state.

### 2.1. Modeling the scattering polarization in C<sub>2</sub> lines

In order to model the Hanle effect in such C<sub>2</sub> lines, we have solved the statistical equilibrium equations (SEE) for the irreducible tensor components,  $\rho_Q^K$ , of the atomic density matrix, considering a realistic multilevel model [see Eq. (7.11) in Landi Degl'Innocenti & Landolfi (2004)]. Our molecular model for C<sub>2</sub> includes levels from  $J=0$  to  $J=120$  of the fundamental vibrational level of both electronic states, including the fine structure due to the spin coupling. Therefore, the number of rotational levels is 360 for each state, giving a total of 720 rotational levels and 2657 radiative transitions. The Einstein coefficients for spontaneous emission,  $A_{ul}$ , have been obtained from Kurucz (1993). The use of this complex molecular model is motivated by the special structure of the radiative transitions in C<sub>2</sub>. The stronger transitions are those of the P ( $\Delta J = J_u - J_l = -1$ ) and R ( $\Delta J = 1$ ) branches. This particular radiative structure produces very strong

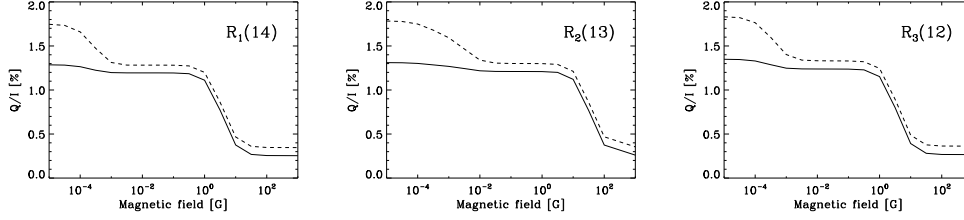


**Fig. 1.** Variation of the calculated fractional linear polarization amplitude,  $Q/I$ , with the strength of the assumed micro-turbulent magnetic field for the  $R_1(14)$ ,  $R_2(13)$  and  $R_3(12)$  lines. Note that the critical field of the  $R_2(13)$  line is more than an order of magnitude larger than that corresponding to the  $R_1(14)$  and  $R_3(12)$  spectral lines. The solid lines are the ones that apply to the observations we have obtained, since they show the computed  $Q/I$  amplitudes when the selective absorption of polarization components produced by the atomic polarization of the lower level (i.e., dichroism) is taken into account, in addition to the selective emission from the polarized upper level. The dashed lines neglect the influence of dichroism, and therefore they are representative of off-limb observations. Interestingly, the lower level Hanle effect can only be detected in the off-limb observation while it is completely masked by the dichroism contribution for the on-disk observation (see Trujillo Bueno, 2003, for a discussion on the interest of on-disk vs. off-limb observations).

*pumping ladders* which couple rotational levels with very different values of  $J$ . These ladders also introduce “boundary effects” because levels close to the boundary of the model (having  $J$  close to 120) are affected by the finite size of the model. We have verified that the results for the rotational levels with  $J \lesssim 40$  become satisfactory for molecular models with a maximum  $J$ -value of 120 (Asensio Ramos & Trujillo Bueno, 2003; Asensio Ramos, 2004).

We consider the effect of a microturbulent and isotropically distributed magnetic field on the linear polarization signal of the  $C_2$  lines. This microturbulent field limit is obtained by solving numerically the SEE for many directions of the magnetic field and then averaging the obtained spherical components of the density matrix. Depolarizing collisions have not been taken into account in the SEE. This is because we have reasons to believe that for the diatomic molecules of the Second Solar Spectrum the important depolarizing collisions are those between different  $J$ -levels pertaining to the same vibrational and electronic state (Trujillo Bueno et al., 2006). However, in homonuclear molecules such as  $C_2$ , very strong selection rules forbid such collisional transitions between different  $J$ -levels

(Herzberg, 1950). It is important to note that if the rates of depolarizing collisions were similar or larger than the Einstein  $A_{ul}$ -coefficient, then the critical magnetic field strength sufficient to produce a significant Hanle effect would be larger than  $B_H$  (Trujillo Bueno et al., 2006).

## 2.2. The line-ratio technique

Fig. 1 shows the magnetic sensitivity of the  $Q/I$  amplitude for each of the lines of the above-mentioned R-triplet. As seen in the figure, the  $Q/I$  amplitude of the  $R_2$  line remains constant for fields weaker than  $\sim 10$  G, while the  $R_1$  and  $R_3$  lines are already approaching the upper-level Hanle saturation regime for  $B > 10$  G. As a consequence, the  $R_2$  lines can be used as reference lines for fields not much stronger than 10 G, while the  $R_1$  (and  $R_3$ ) lines can be used as reference lines for fields above 10 G. In principle, this allows us to diagnose field strengths between 1-100 G.

Fig. 2 shows the variation of the line ratio,  $R_1/R_2$  ( $R_3/R_2$ ), of the corresponding  $Q/I$  amplitudes with the strength of a microturbulent magnetic field. The  $R_1/R_2$  line ratio quickly decreases when increasing the magnetic field

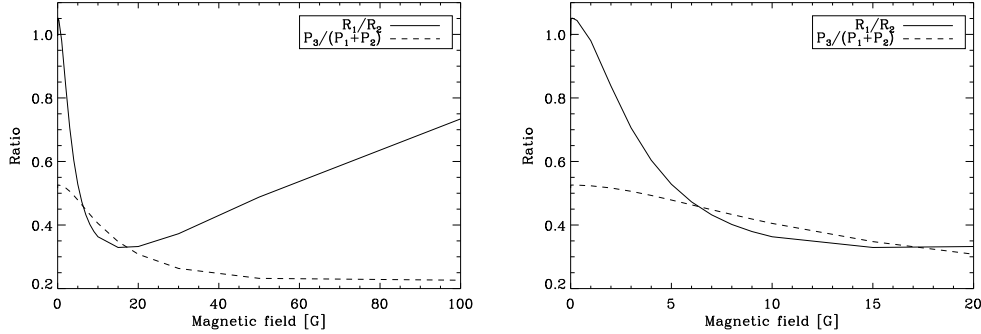


**Fig. 2.** Variation of the ratio  $R_1/R_2$  and  $P_3/(P_1+P_2)$  for increasing values of the intensity of a microturbulent field (left panel). Note that, for a fixed value of the  $R_1/R_2$  ratio, two possible solutions are possible. Fortunately,  $C_2$  lines with  $J > 20$  like the ones used by Trujillo Bueno et al. (2004) indicate that the “weak-field” solution is the correct one. An example of a P-triplet with  $J > 20$  is located in the same spectral region of the chosen R-triplet. The right panel visualizes better the region of interest.

strength until reaching a minimum value for fields of  $\sim 15$  G. This minimum occurs at a magnetic field strength for which the lower level has already reached the Hanle saturation regime, while the upper level Hanle effect starts to be operative for such field strengths ( $\sim 15$  G). Note that, for the R-triplet under consideration, there is not a one-to-one relation between the magnetic field strength and the line ratio. For instance, a ratio of  $1/2$  can be associated with 5 or 50 G. However, as mentioned in the introduction, we already know from the  $C_2$  lines with  $J > 20$  that the weakest-field option is the correct one. For instance, let us consider the  $P_1(42)$ ,  $P_2(41)$  and  $P_3(40)$  lines that can be found in the same spectral window of the observed R-triplet. The magnetic sensitivity of the ratio  $P_3(40)/(P_1(42)+P_2(41))$  is shown by the dashed line of Fig. 2. Although not shown in the plot, this ratio also suffers from an ambiguity, but the maximum possible value of the magnetic field strength is unrealistically high thanks to the fact that the critical Hanle field of the  $P_2(41)$  line is  $B_H \approx 400$  G. This differential behavior between the two triplets can be used to distinguish between the two possible solutions. For instance, for a ratio of 0.3, the two possible values are 20 and 320 G. Since the two ratios have to give a similar field strength

value, the observed ratios restrict the solution to be between 0 and  $\sim 20$  G.

### 3. The Hanle effect in $C_2$ lines: observations

Last June 18 2006, we used THÉMIS to observe the scattering polarization signals of  $C_2$  lines at four positions increasingly closer to the North solar limb. We started doing measurements at an initial position that on the slit-jaw image seemed to be very close to the North solar limb (called Pos=0” in Fig. 3). Afterwards we took two measurements “below” and one measurement “above” that initial reference position, with a space interval of 1.5” between each consecutive pair of observed positions. In all four measurements the intensity profiles of the observed  $C_2$  lines were in absorption, with the Pos=1.5” measurement of Fig. 3 corresponding to the position closest to the North solar limb.

Each measurement was obtained adding up 150 modulation cycles with 600 ms per modulation state. Since we opted for a modulation scheme of 6 measurements per cycle, the total integration time was 540 s. The observations were carried out using the grid technique with the tip-tilt system of THÉMIS working prop-

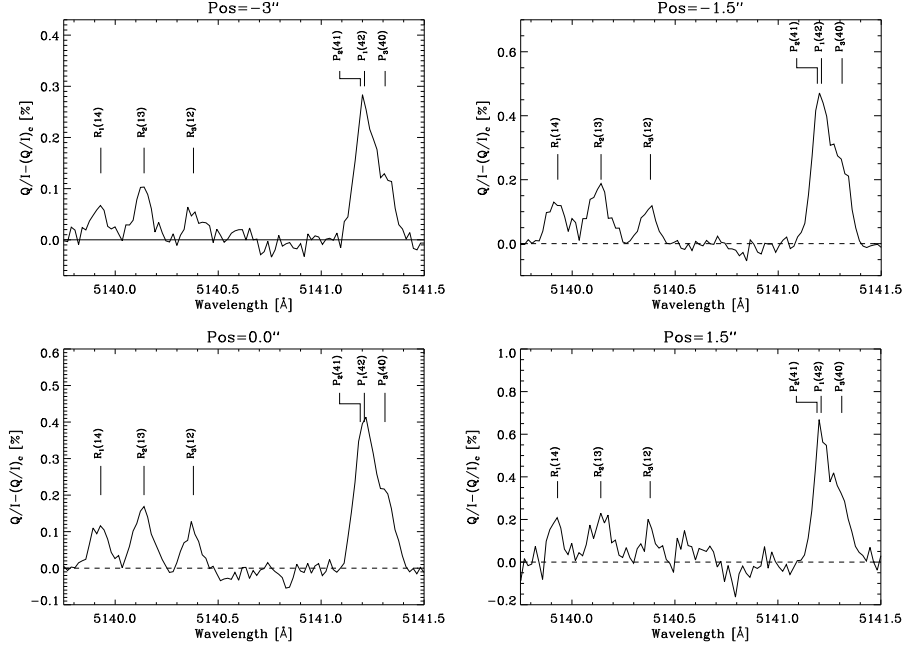


**Fig. 3.** Observed fractional linear polarization profiles at four different positions increasingly close to the North solar limb, after subtracting the continuum polarization level. Note that the  $R_1/R_2$  ratio decreases when approaching the limb, indicating that the strength of the hidden field decreases with height in the solar atmosphere.

erly this time, which allowed us to fix the position of the slit parallel to the solar limb with a precision better than  $0.1''$ . In order to minimize possible misalignments, we only present data from the central part of the slit since the other two parts selected by the grid might be placed at slightly different distances to the limb. The raw data were analyzed with the DeepStokes code (López Ariste et al., 2007), which is based on a spatio-temporal modulation method similar to that reported by Trujillo Bueno et al. (2001). The standard deviation of the noise in the  $Q/I$  measurements is  $\sim 6 \times 10^{-4}$  per pixel. Additional averaging of the signals along the spatial direction of the slit allowed us to increase the signal-to-noise ratio by a factor  $\sim 5$ , thus approaching a polarimetric sensitivity of  $\sim 10^{-4}$ .

The observed  $Q/I$  spectrum is shown in Fig. 3, after having subtracted the continuum polarization level. The observations show

clearly that the three lines of the chosen R-triplet have different amplitudes for the on-disk observations, with the  $R_1$  and  $R_3$  lines giving lower amplitude than the  $R_2$  reference line. Interestingly, the closer to the limb we observe, the smaller the difference between the amplitudes of the  $R_1$  and  $R_3$  lines with respect to the  $R_2$  line. As expected, our observations show also that the amplitudes of the observed  $Q/I$  signals increase when approaching the limb.

The ratio,  $R_1/R_2$ , of the observed polarization amplitudes is close to  $1/2$  at the most distant position from the limb (see top left panel of Fig. 3), while it increases towards 1 when approaching the limb (see the left panel of Fig. 4). In order to improve the significance of our result, we have used both  $R_1/R_2$  and  $R_3/R_2$  ratios, taking into account that they should be similar because the  $R_1$  and  $R_3$  lines have practically the same sensitivity to the magnetic field. The solid line of Fig. 4 gives the ensuing av-

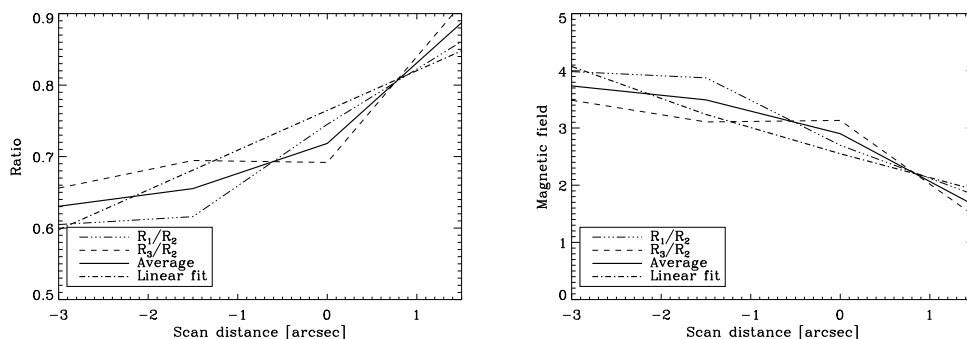


**Fig. 4.** The left panel shows the observed  $R_1/R_2$  and  $R_3/R_2$  ratios at increasingly smaller distances to the limb. Note that the figure also shows the average value and the ensuing linear fit. The right panel shows the variation of the magnetic field strength after using the calibration shown in Fig. 2.

erage, which we take as representative of the height variation of the Hanle-effect line ratio. As seen in the left panel of Fig. 4, it changes from 0.6 to 0.85 when going from the Pos= $-3''$  to the Pos= $1.5''$  of the observations shown in Fig. 3. Thanks to the magnetometry calibration of Fig. 2 the observed variation given in the left panel of Fig. 4 can be interpreted in terms of a height variation of the strength of the inferred hidden field (see the right panel of Fig. 4). As seen in this figure the strength of the hidden field at the atmospheric heights corresponding to the observed positions (which are closer to the solar limb than those of Gandorfer, 2000) varies between 4 G and 2G, decreasing with height in the atmosphere with a gradient of  $\sim 0.5 \text{ G arcsec}^{-1}$ .

*Acknowledgements.* This research has been funded by the Spanish Ministerio de Educación y Ciencia through project AYA2004-05792.

## References

- Asensio Ramos, A. 2004, PhD thesis, Universidad de La Laguna, La Laguna
- Asensio Ramos, A. & Trujillo Bueno, J. 2003, in *Solar Polarization 3*, ed. J. Trujillo Bueno & J. Sánchez Almeida, ASP Conf. Ser. Vol 307, 195
- Berdyugina, S. V. & Fluri, D. M. 2004, *A&A*, 417, 775
- Berdyugina, S. V. & Solanki, S. K. 2002, *A&A*, 385, 701
- Faurobert, M. & Arnaud, J. 2003, *A&A*, 412, 555
- Gandorfer, A. 2000, *The Second Solar Spectrum, Vol. I: 4625 Å to 6995 Å* (Zurich: vdf)
- Herzberg, G. 1950, *Molecular Spectra and Molecular Structure. I. Spectra of Diatomic Molecules* (New York: Van Nostrand Company)
- Kurucz, R. 1993, *Atomic data for opacity calculations (Kurucz CD-ROM No.1)*
- Landi Degl'Innocenti, E. & Landolfi, M. 2004, *Polarization in Spectral Lines* (Kluwer Academic Publishers)
- López Ariste, A., Asensio Ramos, A., Manso Sainz, R., Derouich, M., & Gelly, B. 2007, *A&A*, in preparation
- Stenflo, J. O. & Keller, C. U. 1997, *A&A*, 321, 927
- Trujillo Bueno, J. 2003, in *Solar Polarization 3*, ed. J. Trujillo Bueno & J. Sánchez Almeida, ASP Conf. Ser. Vol 307, 407
- Trujillo Bueno, J., Shchukina, N., & Asensio Ramos, A. 2004, *Nature*, 430, 326
- Trujillo Bueno, J., Asensio Ramos, A., & Shchukina, N. 2006, in *Solar Polarization 4*, ed. R. Casini & B. W. Lites, ASP Conf. Ser., in press
- Trujillo Bueno, J., Collados, M., Paletou, F., & Molodij, G. 2001, in *ASP Conf. Ser. 236: Advanced Solar Polarimetry – Theory, Observation, and Instrumentation*, ed. M. Sigwarth, 141